The American Society of Mechanical Engineers

*Reprinted From*
**FED—Vol. 121, Gas—Solid Flows**
**Editors: D.E. Stock, Y. Tsuji,**
**J. T. Jurewicz, M. W. Reeks, and M. Gautam**
**Book No. G00609 — 1991**

# NUMERICAL SIMULATION OF GAS-SOLID TWO-PHASE FLOW IN A VERTICAL PIPE: ON THE EFFECT OF INTER-PARTICLE COLLISION

**T. Tanaka and Y. Tsuji**
Faculty of Engineering
Osaka University
Osaka, Japan

## ABSTRACT

This paper concerns a Lagrangian simulation method of the gas-solid flow with consideration of inter-particle collision. A fully developed vertical flow was dealt with in the calculation where periodic boundaries were used for saving the number of particles. Calculation of inter-particle collision was carried out using the uncoupling technique. Profiles of macroscopic quantities such as particle velocities and concentrations were obtained and compared with measurements. The calculated results agreed well with experiments. Also, it was found that the inter-particle collision has a large effect on the diffusion of particles even at a small particle concentration.

## 1. INTRODUCTION

There are two approaches for the numerical simulation of gas-solid flows regarding the treatment of the solid phase. One is the Eulerian method and the other is the Lagrangian method. In general the Eulerian method, in which the solid phase is treated as a continuum like a fluid, is not suitable for large and heavy particles. Trajectories of individual particles are pursued in the Lagrangian method which is applicable not only to the case of small particles but also to the case of large particles having large inertia. It should be noted as advantage of the Lagrangian method that particle-to-wall and particle-to-particle interactions can be taken into account based on the physical properties of materials concerned.

For small particles, gas turbulence has a predominant effect on particle diffusion. Models of diffusion due to gas turbulence have been developed by some researchers like Elghobashi & Abou-Arab (1983) and Chen & Wood (1985) for example. Gas turbulence is not influential for large solid particles, and other effects such as rebound on the wall or particle-to-particle interaction are important. Matsumoto & Saito (1970) and Tsuji et al. (1989a,b) performed simulations without considering inter-particle collision in a horizontal channel. They attributed the particle diffusion to irregular bouncing on a wall caused by nonsphericity of particle. However it is hard to think that the local particle concentration in their results is low enough to neglect the inter-particle collision. Lourenco et al. (1983) deduced a kinetic model of gas-particle flows from the similarity of particle motion to that of molecules in rarefied gas. They used the Boltzmann equation with the collision term and calculated a horizontal flow at low particle loading. They showed that the inter-particle collision plays an important role even in the case of dilute phase flows. Kitron et al. (1990) applied the direct simulation Monte Carlo (DSMC) method to a gas-solid flow in impinging stream reactors. The DSMC method has been developed by Bird (1976) for solving the Boltzmann equation numerically.

In this paper a Lagrangian simulation method with inter-particle collision is presented for the fully developed gas-solid flow in a vertical pipe. It is assumed that particles do not change the gas flow except for the additional pressure loss and turbulent diffusion due to gas is negligible. Calculation of inter-particle collision is carried out using the uncoupling technique mentioned later. Periodic boundaries are set up as the inlet and the outlet of the calculation region of interest to reduce the number of particles calculated. In the section of results, effects of the solid loading on particle concentration and velocity profiles are investigated. Furthermore the results are compared with experiments by Tanaka et al. (1989).

## 2. GENERAL ASPECT

### 2.1 Simulation procedure

The algorithm of the inter-particle collision is a key point in this work, because it greatly affects the computation time. The present authors followed the well-known technique developed by Bird (1976); that is, the collision is calculated separately from calculation of particle motion. In this technique of uncoupling, the time step in a finite difference algorithm is taken to be small compared with the mean free time. The mean free time $\tau$ is evaluated by $\tau = \lambda/|\bar{v}_p'|$, where $|\bar{v}_p'|$ is the local mean particle velocity fluctuation.

The calculation was carried out by repeating the following procedure:

(a) First, motions of all particles in the time interval $\Delta t$ are calculated by the equations of motion. If the particle collides with the wall, the velocities after rebound on the wall are calculated. The velocity after the time step $\Delta t$ is called "new velocity" in this

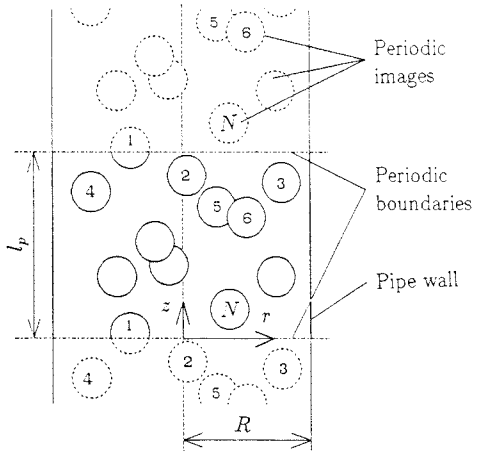


Fig. 1 Calculation region

paper.

(b) Next, occurrence of inter-particle collisions in the step $\Delta t$ is examined as shown later in detail. If a particle is decided to collide with another particle, the post-collision velocities of the collision pair are calculated by the impulsive equations where the "new velocities" are regarded as the velocities before inter-particle collision. Some particles rebounding on the wall collide with other particles during the time step $\Delta t$. If rebound takes place before the inter-particle collision, the new velocity is used in the same way as the above. If rebound takes place after the inter-particle collision, the "old velocity" is used to calculate the post-collision velocities. In this case, the motion of particles of the collision pair in the time step $\Delta t$ is re-calculated using the post-collision velocities.

## 2.2 Calculation region

It is difficult in practice to consider an actual pipe length, because a great number of particles should be dealt with. Therefore in this work a fully developed flow region bounded by periodic boundaries, as shown in Fig.1, is considered to limit the number of particles calculated. The periodic boundaries are regarded as the inlet and the outlet of the calculation region. A particle going out through one periodic boundary returns the other with the same position and velocity. Hence the number of particles in the region remains constant. If the number of particles is fixed, the solid concentration can be adjusted arbitrarily by varying the distance between the periodic boundaries. The mean solid volume fraction $\rho_{vO}$ in the region is given by

$$\rho_{vO} = \left(\sum_{i=1}^{N} V_{pi}\right) / (\pi R^2 l_p), \tag{1}$$

where $V_{pi}$ is the volume of the $i$-th particle, $N$, the number of particles in the region, $R$, the pipe radius, and $l_p$ is the distance between periodic boundaries.

Generally the mean component of particle velocity (axial) is much larger than fluctuating components which are more important when considering the inter-particle collision. If a particle moves downstream with its axial velocity, it goes too far from the region of calculation accompanying the stationary periodical boundaries. Therefore in this work, we let the periodical boundary move with the same velocity as the mean particle velocity.

The influence of $l_p$ on the results was investigated in the preliminary calculation. Regarding the influence of $l_p$, the work by Campbell and Brennen (1985) is referred to. They calculated the chute flow with the periodic boundaries and found that the influence of $l_p$ is negligible if $l_p$ is greater than five times of the particle diameter. However their criterion is not applicable to the present condition, since the particle concentration in their calculation is much higher than that of the present work. The particle phase is so dilute in the present flow that another measure than the particle diameter should be used. It is reasonable to adopt the mean free path as such a measure. The mean free path is given by

$$\lambda = (\sqrt{2}\pi\ d_p^2 n)^{-1}, \tag{2}$$

where $d_p$ is the particle diameter and $n$ is the number density of particles given by

$$n = N / \left(\frac{\pi}{4} D^2 l_p\right). \tag{3}$$

Substituting equation (3) into (2) yields

$$l_p/\lambda = 4\sqrt{2}(d_p/D)^2 N. \tag{4}$$

This equation means that $l_p/\lambda$ is decided by $N$. It was confirmed in the preliminary calculation that the effect of the periodic boundary is negligible if $l_p/\lambda$ is sufficiently large.

## 2.3 Equation of motion for particles

Calculations were carried out under the following assumptions: (a) Particles are rigid spheres, (b) The particle concentration is so low that the gas velocity distribution is not affected by solid particles, (c) The particle diffusion due to gas turbulence is negligible.

The equation of particle motion is given by

$$m\frac{d\boldsymbol{v}_p}{dt} = C_D\frac{1}{2}\rho\boldsymbol{u}_R|\boldsymbol{u}_R|S_p + C_{LR}\frac{1}{2}\rho|\boldsymbol{u}_R|\frac{\boldsymbol{u}_R\times\boldsymbol{\omega}}{|\boldsymbol{\omega}|}S_p + \boldsymbol{F}_{LG} + \boldsymbol{F}_g \tag{5}$$

where $m$ is particle mass, $\boldsymbol{v}_p$, particle velocity, $C_D$, drag coefficient, $\rho$, gas density, $S_p$, projected area of a particle, $C_{LR}$, lift coefficient due to particle rotation, $\boldsymbol{\omega}$, particle rotational velocity, and $\boldsymbol{u}_R$ is gas velocity relative to a particle. The first term in the right side of Eq.(5) expresses the drag force, the second term, the Magnus lift force, $\boldsymbol{F}_{LG}$, the lift force due to velocity gradient and $\boldsymbol{F}_g$ is the gravitational force. The expression given by Morsi and Alexander (1972) was used for $C_D$. The following expression was assumed for $C_L$ based on a few experiments for middle and high Reynolds number.

$$C_L = \min(0.5, 0.5\frac{a\omega}{|u_R|}). \tag{6}$$

where $a$ is the particle radius.

For the lift force $\boldsymbol{F}_{LG}$ due to velocity gradient, the Saffman's theoretical result (Saffman,1965,1968) was considered. In the present condition only the $r$ component of $\boldsymbol{F}_{LG}$ remains because of axisymmetry of gas velocity profile.

$$F_{LGr} = 1.62 u_{Rz} d_p^2 \sqrt{\rho\mu\frac{du_{Rz}}{dr}}\frac{du_{Rz}/dr}{|du_{Rz}/dr|}, \tag{7}$$

where $u_{Rz}$ is the $z$ component of $\boldsymbol{u}_R$.

The equation of rotational motion of a particle is expressed as

$$I\frac{d\boldsymbol{\omega}}{dt} = -M\frac{1}{2}\rho a^5|\boldsymbol{\omega}|\boldsymbol{\omega}, \tag{8}$$

where $I$ is the moment of particle inertia. The right side of equation(8) is the viscous torque against the particle rotation, which is theoretically obtained by Dennis et al. (1980) and Takagi (1977). $M$ is the non-dimensional coefficient determined by $Re_R = |\boldsymbol{\omega}|d_p^2/(4\nu)$ which is the rotational Reynolds number defined by $Re_R = |\boldsymbol{\omega}|d_p^2/(4\nu)$.

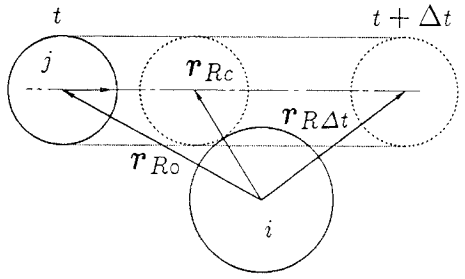


Fig. 2 Occurrence of Inter-particle collision

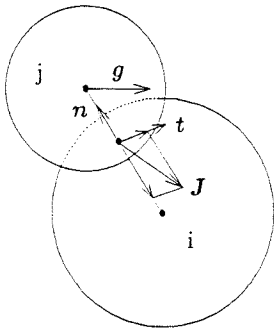


Fig. 3 Inter-particle collision

## 2.4 Inter-particle collision

The particle concentration is so low in the present work that binary collision, as shown in Fig. 2, is assumed to be overwhelming. The procedure of examining whether inter-particle collision occurs is as follows. Let us consider particles $i$ colliding with particle $j$ during one time step $\Delta t$. $\boldsymbol{r}_o$ is the position vector at time $t$ and $\boldsymbol{r}_{\Delta t}$ is the position vector after $\Delta t$. The subscripts '$i$' and '$j$' are added to the quantities relating to each particle. Each particle is assumed to do a linear motion with a constant velocity from $\boldsymbol{r}_o$ to $\boldsymbol{r}_{\Delta t}$. Fig. 2 shows the relative motion of particle $j$ to $i$, where $\boldsymbol{r}_R = \boldsymbol{r}_j - \boldsymbol{r}_i$, is the relative position vector. The relative distance between the two particles is given by $|\boldsymbol{r}_R + k(\boldsymbol{r}_{\Delta t} - \boldsymbol{r}_o)|$, where $k$ represents a non-dimensional time normalized by $\Delta t$. The condition required for the collision during this time step is that the following equation of $k$,

$$|\boldsymbol{r}_{R0} + k(\boldsymbol{r}_{R\Delta t} - \boldsymbol{r}_{Ro})|^2 = (a_i + a_j)^2, \tag{9}$$

has two real roots $k_1$ and $k_2$ ($k_1 < k_2, 0 \leq k_1 < 1$). The relative position vector of the collision is give by

$$\boldsymbol{r}_{Rc} = \boldsymbol{r}_{R0} + k_1(\boldsymbol{r}_{R\Delta t} - \boldsymbol{r}_{Ro}). \tag{10}$$

When inter-particle collision occurs, the post-collision velocities of the collision couples are calculated by the equations of impulsive motion with some assumptions. Details of the calculation process are as follows. Equations of impulsive motion are given by

$$\boldsymbol{v}_{pi}^* = \boldsymbol{v}_{pi} + \boldsymbol{J}/m_i, \tag{11}$$

$$\boldsymbol{v}_{pj}^* = \boldsymbol{v}_{pj} - \boldsymbol{J}/m_j, \tag{12}$$

$$\boldsymbol{\omega}_i^* = \boldsymbol{\omega}_i + a_i \boldsymbol{n} \times \boldsymbol{J}/I_i, \tag{13}$$

$$\boldsymbol{\omega}_j^* = \boldsymbol{\omega}_j + a_j \boldsymbol{n} \times \boldsymbol{J}/I_j. \tag{14}$$

In the above equations, $\boldsymbol{n}$ is the normal unit vector directed from the particle $i$ to $j$ and given by $\boldsymbol{n} = \boldsymbol{r}_{Rc}/(a_i + a_j)$, $\boldsymbol{J}$, the impulsive force exerted on the particle $i$, as shown in Fig. 3, and post-collision quantities are asterisked. According to the rule in the section 2.1, the particle velocities and rotational velocities at the time $t$ or $t + \Delta t$ are used for the pre-collision velocities $\boldsymbol{v}_p$ and $\boldsymbol{\omega}$. Next, the slip velocity before the collision is considered. Using the relative velocity

$$\boldsymbol{g} = \boldsymbol{v}_{pj} - \boldsymbol{v}_{pi}, \tag{15}$$

the slip velocity of the particle $j$ to $i$ at the contact point is given by

$$\boldsymbol{g}_{fc} = \boldsymbol{g} - (\boldsymbol{g} \cdot \boldsymbol{n})\boldsymbol{n} - a_i \boldsymbol{\omega}_i \times \boldsymbol{n} - a_j \boldsymbol{\omega}_j \times \boldsymbol{n}. \tag{16}$$

Dividing the impulsive force $\boldsymbol{J}$ into the normal and the tangential components,

$$\boldsymbol{J} = J_n \boldsymbol{n} + J_t \boldsymbol{t}. \tag{17}$$

Since the friction force is in the direction of slip velocity, $\boldsymbol{t}$ is expressed as

$$\boldsymbol{t} = \boldsymbol{g}_{fc}/|\boldsymbol{g}_{fc}|. \tag{18}$$

The normal components of relative velocities $\boldsymbol{g}$ and $\boldsymbol{g}*$ are related to each other through the coefficient of restitution $e_p$ as follows.

$$\boldsymbol{n} \cdot \boldsymbol{g}* = -e_p(\boldsymbol{n} \cdot \boldsymbol{g}) \tag{19}$$

From equations (11),(12),(15),(17) and (19), $J_n$ is derived as

$$J_n = \frac{(1+e)\boldsymbol{n} \cdot \boldsymbol{g}}{1/m_i + 1/m_j}. \tag{20}$$

From equations (11) $\sim$ (17), the slip velocity after the collision is obtained by

$$\boldsymbol{g}_{fc}* = \alpha \boldsymbol{t}, \tag{21}$$

$$\alpha = |\boldsymbol{g}_{fc}| - \frac{7}{2}\left(\frac{1}{m_i} + \frac{1}{m_j}\right) J_t. \tag{22}$$

The Coulomb's friction law was used for the tangential impulsive force during the slip motion.

$$J_t = -\mu_{fp} J_n, \tag{23}$$

where $\mu_{fp}$ is the coefficient of kinetic friction between particles. Equation (23) is valid only for positive $\alpha$. Substituting equation (23) into equation (22) and putting $\alpha \geq 0$,

$$J_n \geq \frac{-2|\boldsymbol{g}_{fc}|}{7\mu_{fp}(1/m_i + 1/m_j)}. \tag{24}$$

If equation (24) is satisfied, $J_t$ is given by equation (23). If equation (24) is not satisfied, the slip at the contact point stops in the period of collision. Assuming that slip does not occur again after the initial slip dies out and substituting $\alpha = 0$ into equation (22), we get

$$J_t = \frac{2|\boldsymbol{g}_{fc}|}{7(1/m_i + 1/m_j)}. \tag{25}$$

The impulsive force was obtained by equations (20), (24), (23) and (25), and the post-collision velocities and rotational velocities were obtained by equations (11) $\sim$ (14).

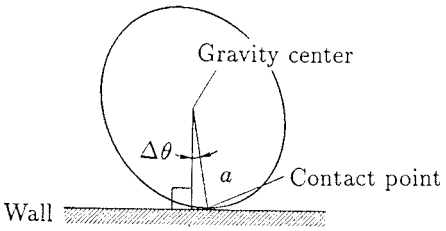


Fig. 4 Contact with a wall

Table 1 Calculation condition

| | | |
|---|---|---|
| Time step $\Delta t$ (s) | $2\times10^{-3}$ | |
| Pipe inner diameter $D$(mm) | 40 | |
| Mean gas velocity $U$(m/s) | 16 | |
| Gas density $\rho$(kg/m$^3$) | 1.205 | |
| Kinematic viscosity $\nu$(m$^2$/s) | $1.515\times10^{-5}$ | |
| Mean particle diameter $d_p$(mm) | 0.406 | 1.50 |
| Particle density (kg/m$^3$) | 1038 | 1032 |
| Coefficient of restitution between particles $e_p$ | 0.94 | 0.94 |
| Coefficient of restitution between particle and wall | 0.94 | 0.94 |
| Coefficient of kinetic friction between particles $\mu_{fp}$ | 0.325 | 0.279 |
| Coefficient of kinetic friction between particle and wall | 0.325 | 0.279 |
| $\Delta\theta_{max}$ (deg) | 2 | 2 |
| Number of particles in the calculation region $N$ | 800 | 200 |
| $l_p/\lambda$ | 0.466 | 1.59 |
| Relaxation distance $l_r$ (m) | 0.295 | 3.22 |

### 2.5 Rebound of a particle on a wall

Some previous researchers (Matsumoto and Saito, 1970; Tsuji et al., 1989a, b) have shown that irregular bouncing of a particle on a wall which is caused by deviation of particle shape from "perfect" sphere plays an important role for the particle motion in horizontal flows. Therefore the irregular bouncing was considered in this work. Several models have been proposed to express the irregular bouncing. Matsumoto and Saito (1970) made an ellipsoid model. Tsuji et al. (1989a, b) dealt with particles having arbitrary shapes. Irregular bouncing with a smooth wall in these models is caused by the same mechanism; that is, the contact point of the particle with the wall does not coincide with the foot of a perpendicular from the gravity center of the particle. Irregular bouncing can be produced artificially by adjusting the deviation angle $\Delta\theta$ as shown in Fig. 4. In the present calculation the deviation angle was given by random numbers ranged uniformly from 0 to $\Delta\theta_{max}$. Following actual particles in the experiment for comparison with the calculation, particles were assumed to be nearly spherical. Hence let the distance between the gravity center and the contact point constant like a sphere. Tsuji et al. (1989a) solved the equations of impulsive motion for a non-spherical body rebounding on a plane wall. Their solution is restricted to two dimensional collision in which the direction of rotational velocity of particle is parallel to the wall and perpendicular to the particle velocity. The solutions given by Tsuji et al. (1989a) were extended to three dimensional collision here.

## 3. RESULTS

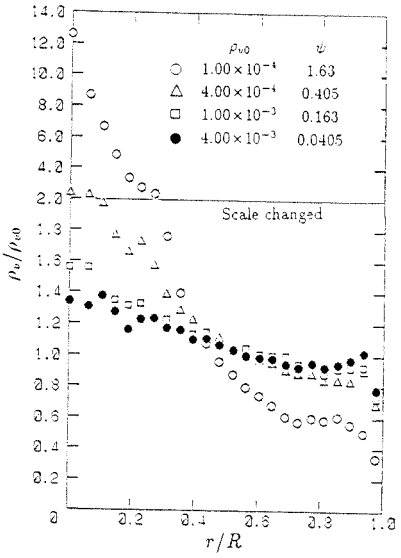


Fig. 5 Effect of particle loading on the concentration distribution ($\bar{d}_p = 0.406$ mm)

### 3.1 Calculation condition

Table 1 shows the calculation conditions, which are given referring to experiments (Tanaka et al., 1989) served for comparison. An acrylic pipe and polystyrene particles were used in the experiments. The coefficients of restitution and friction between the particle and wall were the measured value. However the coefficients between the particles were assumed to be the same as those between the particle and wall for simplicity. Particle size distributions were given according to the experiment. $\Delta\theta_{max}$ was evaluated roughly from observations of rebound motion of particles falling vertically on a horizontal plane wall. Although the value of $\Delta\theta$ is small, it is sufficient to express the random walk on a horizontal wall.

As a result of the preliminary calculation, it was found that the effect of periodic boundaries was not observed for $l_p/\lambda > 0.1$ in the 0.4mm particles and for $l_p/\lambda < 0.3$ in the 1.5mm particles. From these results $N$ is given as shown in table 1.

The relaxation distance is defined by $l_r = v_t^2/g$, where $v_t$ is the terminal velocity.

### 3.2 Concentration distributions

The effect of particle loading on the concentration distribution is shown in Figs. 5 and 6, where $\rho_v$ is the solid volume fraction, $\rho_{v0}$ is the mean value of $\rho_v$ as shown in equation (1), and $\psi$ is the parameter defined by $\psi = \lambda/l_r$. When $\psi$ is large, velocity fluctuations yielded by inter-particle collision decay before the next collision. Therefore $\psi$ can be regarded as a measure representing the effect of particle diffusion due to inter-particle collision.

When $\rho_{v0}$ is low or $\psi$ is large, particles tend to concentrate to the pipe axis owing to the lift force due to velocity gradient. This tendency leads to an extreme results which we confirmed in the calculation without the inter-particle collision, that is, all the particles asymptotically approach to the pipe axis. If we consider the turbulent diffusion, which is omitted in the present simulation, it is possible to avoid such an extreme result.

The concentration profile becomes flatter with decreasing $\psi$, but change in the concentration profile caused by $\psi$ is different according to the particle size. In the case of the 0.4 mm particles the profile becomes flatter monotonously with $\psi$, while it is not monotonous in the 1.5 mm particles. This tendency is consistent with the results of the fluctuating component of particle velocity shown in the following section.

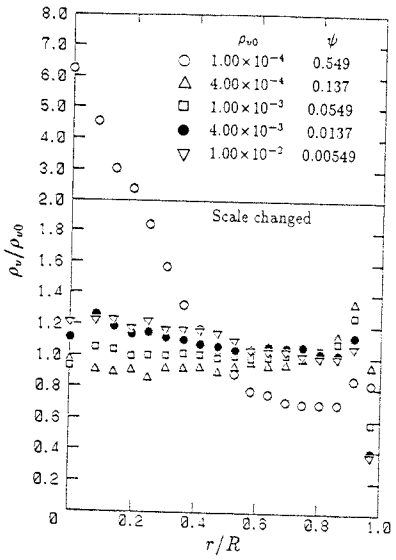


Fig. 6 Effect of particle loading on the concentration distribution ($\bar{d}_p = 1.50$ mm)

An attention was paid to particle trajectories to investigate the high particle concentration near the pipe wall at high $\psi$, which is observed in Fig. 6. A particle having large peripheral velocity loses the radial velocity through repeated inelastic collision with the pipe wall, and gradually is in spiral motion along the pipe wall. On the other hand, when $\psi$ is small, frequent inter-particle collisions prevent particles from making such a spiral motion.

Calculated distributions are compared with experiments (Tanaka et al.1989) in Figs. 7 and 8, where a good agreement is observed.

### 3.3 Particle velocity profiles

Figs. 9 and 10 show the particle velocity distribution. In these figures $\bar{v_{pz}}$ is the local mean particle velocity in the direction of the pipe axis, and $\sqrt{\bar{v_{pz}'^2}}$ and $\sqrt{\bar{v}_{pc}^2}$ are local velocity fluctuations parallel and perpendicular to the pipe axis, respectively. $\sqrt{\bar{v}_{pc}^2}$ represents the intensity of particle diffusion. Experimental results (Tanaka et al.1989) are presented in the figures for comparison.

Since the component of diffusion velocity $\sqrt{\bar{v}_{pc}^2}$ tends to dissipate owing to the drag force, the kinematic energy must be supplied to that component if the diffusion velocity is maintained. The present simulation shows that this kinematic energy is supplied from $\sqrt{\bar{v}_{pz}'^2}$ through the inter-particle collision process. When the solid loading is small, $\sqrt{\bar{v}_{pc}^2}$ is smaller than $\sqrt{\bar{v}_{pz}'^2}$. This is because of less frequency of inter-particle collision. As the solid loading increases, the profiles of $\sqrt{\bar{v}_{pz}'^2}$ and $\sqrt{\bar{v}_{pc}^2}$ become nearly uniform in the pipe cross section and the difference between them decreases because of increasing inter-particle collisions. The effects of inelasticity and friction in inter-particle collision are not remarked in low or moderate solid loading but as the loading increases, those effects come about. In fact, Fig. 10(c) shows reduction of fluctuating velocity. If the solid loading increases further in the case of Fig. 9, the same reduction of fluctuating velocity as Fig. 10(c) is expected to appear. The above results of $\sqrt{\bar{v}_{pc}^2}$ exactly correspond to the change in the concentration profile. The more $\sqrt{\bar{v}_{pc}^2}$, the more uniform the concentration profile.

Next, the calculated results are compared with experiments for the mean velocity. The calculation agrees well with the experiment except the case of $\rho_{vO} \approx 2 \times 10^{-3}$ of the 1.5 mm particles in which the calculated velocity is a little smaller than the experiment.

The present authors consider that the above disagreement is caused by the coefficient of friction between the particle and wall used in the calculation. The friction coefficient used in the calculation is based on a measurement with clean particles and clean wall, but actual value of the coefficient is reduced by contamination.

It is found from these results that the intensity of $\sqrt{\bar{v}_{pc}^2}$ has significant effects on the concentration distributions. So far very few attention has been paid to $\sqrt{\bar{v}_{pc}^2}$ and there have been scarce data about $\sqrt{\bar{v}_{pc}^2}$. For further understanding gas-solid flows in the pipe, measurements of $\sqrt{\bar{v}_{pc}^2}$ are required and the effect of it on other quantities should be clarified experimentally.

## 4. CONCLUSION

A numerical simulation method with inter-particle collision for gas-solid two-phase flow is presented, and the fully developed flow of inertia predominant particles in a vertical pipe was predicted. The obtained results are summarized as follows:

(1) Irregular bouncing is not effective enough to produce particle diffusion in a vertical pipe.

(2) Inter-particle collision have a decisive effect on the particle diffusion even at a small solid loading.

(3) The present results compare well the experiments (Tanaka et al., 1989) for distributions of solid concentration and velocity.

## ACKNOWLEDGMENTS

The authors are grateful to Mr. K. Kadono for his assistance with the present work.

## REFERENCES

Bird, G. A., 1976, "Molecular Gas Dynamics," Clarendon, Oxford.

Campbell, C. S., and Brennen, C. E., 1985, "Chute Flows of Granular Material: Some Computer Simulations," ASME *Journal of Applied Mechanics*, Vol. 52, pp. 172-178.

Chen, C. P. and Wood, P. E., "A Turbulence Closure Model for Dilute Gas-Particle Flows," *Canadian J. Chem. Engng.*, Vol. 63, Jun. 1985, pp. 349-360.

Dennis, S. C. R., Singh, S. N. and Ingham, D. B., 1980, "The Steady Flow due to a Rotating Sphere at Low and Moderate Reynolds Number," *Journal of Fluid Mechanics*, Vol. 101, pp. 257-270.

Elghobashi, S. E. and Abou-Arab, T.W., 1983, "A Two-EquationTurbulence Model for Two-Phase Flows," *Physics of Fluids*, Vol 26, pp. 931-938.

Kitron, A., Elperin, T., and Tamir, A., 1990, "Monte Carlo Simulation of Gas-Solids Suspension Flows in Impinging Streams Reactors," *International Journal of Multiphase Flow*, Vol.16, No. 1, pp. 1-17.

Lourenco, L., Riethmuller, M. L., and Essers, J-A, 1983, "The Kinetic Model for Gas Particle Flow and Its Numerical Implementation," *Proceedings, International Conference on the Physical Modeling of Multi-Phase Flow*, BHRA Fluid Engineering, Cranfield, U.K., pp. 501-525.

Matsumoto, S., and Saito, S., 1970, "On the mechanism of Suspension of Particles in Horizontal Pneumatic Conveying: Monte Carlo Simulation Based on the Irregular Bouncing Model," *Journal of Chemical Engineering of Japan*, Vol. 3, No. 1, pp. 83-92.

Morsi, S. A. and Alexander, A. J., 1972, *Journal of Fluid Mechanics*, Vol. 55, Part.2, pp. 193-208.

Saffman, P. G., 1965, "The Lift on a Small Sphere in a Slow Shear Flow,", 1972, Vol. 22, Part 2, pp. 385-400; 1968, Vol. 31, p. 624.

Takagi,H., 1977, "Viscous Flow Induced by Slow Rotation of a Sphere," *Journal of the Physical Society of Japan*, Vol. 42, pp. 319-325.

Tanaka, et al., 1989, "Measurements of Gas-Solid Two-Phase Flow in a Vertical Pipe,(in Japanese)" *Transactions of JSME*, ,Vol. 55, No. 516, B, pp. 2302-2309.

Tsuji, Y., Shen, N. Y., and Morikawa, Y., 1989a, "Numerical Simulation of Gas-Solid Flows. 1: Particle-to-Wall Collision," Technology Reports of the Osaka Univ., Vol. 39, pp. 233-241.

Tsuji, Y., Shen, N., Y., and Morikawa, Y., 1989a, "Numerical Simulation of Gas-Solid Flows. 2: Calculation of a Two-Dimensional Horizontal Channel Flow," Technology Reports of the Osaka Univ., Vol. 39, pp. 243-254.

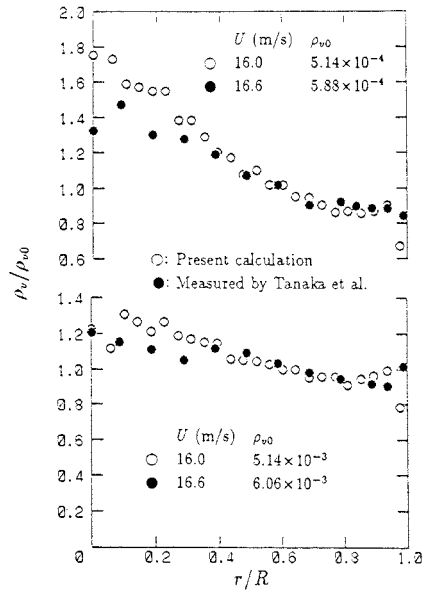


Fig. 7 Comparison of the concentration distribution between the calculation and measurement ($\bar{d}_p$ = 0.406 mm)

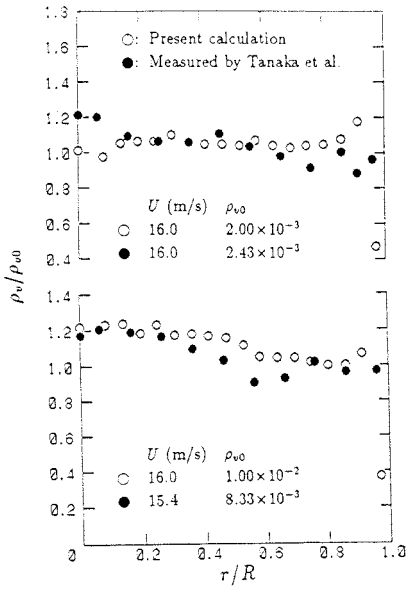


Fig. 8 Comparison of the concentration distribution between the calculation and measurement ($\bar{d}_p$ = 1.50 mm)

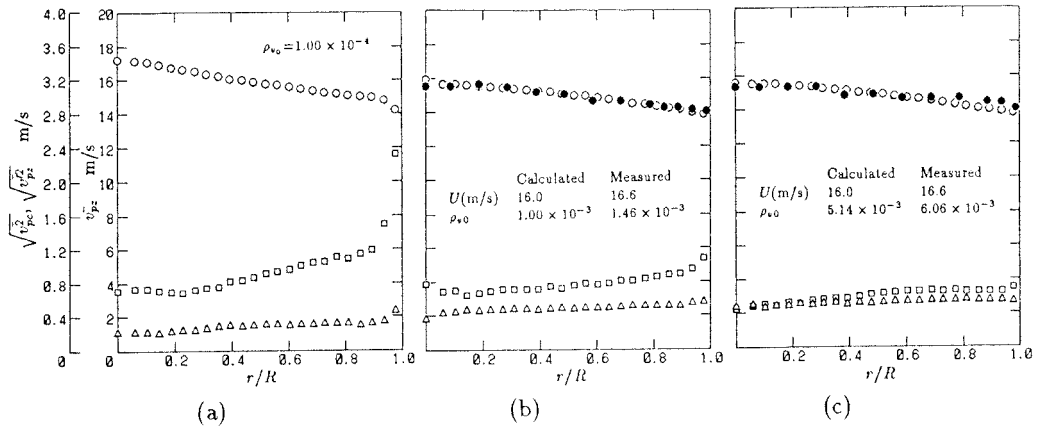


Fig. 9 Distributions of the particle velocity and velocity fluctuation ($\bar{d}_p$ = 0.406 mm ; Present calculation ○ : $v_{pz}^-$, □ : $\sqrt{v_{pz}'^2}$, △ : $\sqrt{v_{pc}^2}$ ; Measured by Tanaka et al. (1989) ● : $v_{pz}^-$)

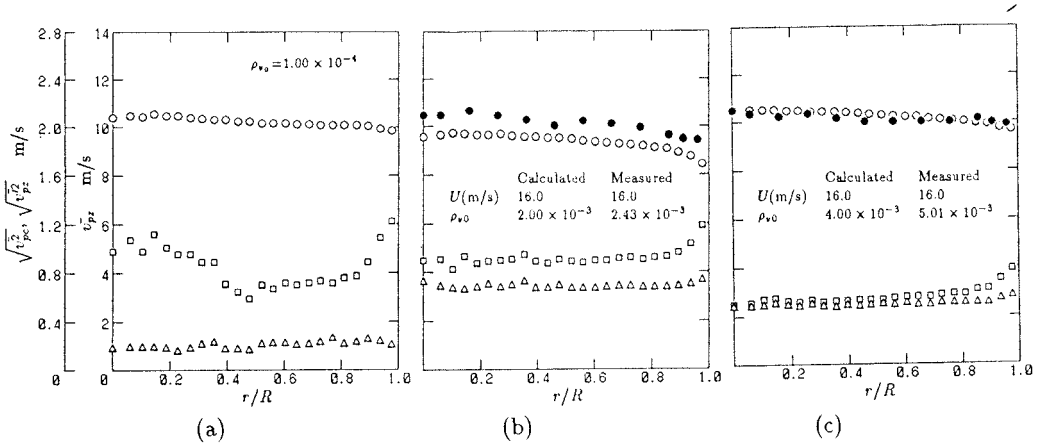


Fig. 10 Distributions of the particle velocity and velocity fluctuation ($\bar{d}_p$ = 1.50 mm ; For legend, see Fig. 9 )